

● *Original Contribution*

ULTRASOUND SPECKLE TRACKING STRAIN ESTIMATION OF *IN VIVO* CAROTID ARTERY PLAQUE WITH *IN VITRO* SONOMICROMETRY VALIDATION

ERIK WIDMAN,* KENNETH CAIDAH,† BRECHT HEYDE,‡ JAN D'HOOGHE,‡ and MATILDA LARSSON*‡

*Department of Medical Engineering, School of Technology and Health, KTH Royal Institute of Technology, Stockholm, Sweden; †Department of Molecular Medicine and Surgery, Karolinska Institutet, Stockholm, Sweden; and ‡Cardiovascular Imaging & Dynamics, Department of Cardiovascular Sciences, KU Leuven, Leuven, Belgium

(Received 11 April 2014; revised 3 June 2014; in final form 23 June 2014)

Abstract—Our objective was to validate a previously developed speckle tracking (ST) algorithm to assess strain in common carotid artery plaques. Radial and longitudinal strain was measured in common carotid artery gel phantoms with a plaque-mimicking inclusion using an in-house ST algorithm and sonomicrometry. Moreover, plaque strain by ST for seven patients (77 ± 6 y) with carotid atherosclerosis was compared with a quantitative visual assessment by two experienced physicians. *In vitro*, good correlation existed between ST and sonomicrometry peak strains, both radially ($r = 0.96$, $p < 0.001$) and longitudinally ($r = 0.75$, $p < 0.01$). *In vivo*, greater pulse pressure-adjusted radial and longitudinal strains were found in echolucent plaques than in echogenic plaques. This illustrates the feasibility of ultrasound ST strain estimation in plaques and the possibility of characterizing plaques using ST strain *in vivo*. (E-mail: erik.widman@sth.kth.se) © 2015 World Federation for Ultrasound in Medicine & Biology.

Key Words: Carotid artery, *In vitro*, *In vivo*, Phantom, Plaque characterization, Speckle tracking, Strain, Ultrasound, Validation.

INTRODUCTION

Plaque characterization is critical when determining treatment for patients with carotid atherosclerotic plaque (Mono et al. 2012; Reid 1998). One type of plaque, known as vulnerable plaque, has a high probability of rupture, which causes emboli to break off from the plaque and travel *via* the circulatory system to vessels in the brain. As the arteries become narrow, the emboli can lodge in the vessel wall, restricting blood flow to parts of the brain and causing a temporary transient ischemic attack or permanent embolic stroke (Reckless and Buchan 2008). Plaque characterization in the carotid artery is therefore significant in risk assessment for cerebral ischemic events.

In current clinical practice, ultrasound-based methods for plaque characterization are limited to visual assessment of plaque morphology, hypo-echoic area and echo reflection in the plaque (Gray-Weale et al. 1988; Kakkos et al. 2013) or, more commonly in research, computerized

evaluation of echogenic properties (Prah et al. 2010). Limitations of visual assessment include inter-observer variability, human error and misclassification caused by ultrasound machine settings (Arnold et al. 1999). Other clinical practices for carotid plaque detection include carotid angiography (Armas et al. 1981; Matos et al. 2014), although angiography determines only plaque location and size and does not offer information on plaque composition. Treatment options such as endarterectomy and angioplasty are often based on relative lumen diameter. The accepted criterion for surgical selection of patients with symptomatic carotid artery disease is a stenosis of 70% reduction in relative lumen diameter of the internal carotid artery (Arnold et al. 1999). In certain instances of plaque composition, location and luminary occlusion, surgery poses a higher risk to the patient than non-invasive treatments such as medication (Easton and Wilterdink 1994). Quantitative tools are needed to better assess the likelihood of plaque rupture to determine if invasive treatment options are required, particularly in cases with borderline lumen obstruction.

Plaque characterization has been attempted with a number of imaging modalities and techniques. Magnetic resonance imaging (MRI) has been used to characterize

Address correspondence to: Erik Widman, School of Technology and Health, KTH Royal Institute of Technology, Alfred Nobels Allé 10, 141 52 Huddinge, Sweden. E-mail: erik.widman@sth.kth.se

plaque, but is expensive and time consuming and can be a high risk factor in initiating recurrent plaque rupture events (Ronen et al. 2007; Teng et al. 2011; Zhao et al. 2013). Saba et al. (2013) attempted to use computed tomography (CT) to characterize plaque based on Hounsfield unit (HU) values, but found that the plaque HU level significantly changed with the kilo-electron volts applied.

Non-invasive ultrasound-based methods include measuring the gray-scale median (GSM) of plaques (Biasi et al. 1999; Kanber et al. 2013a; Salem et al. 2012), although conflicting studies question the effectiveness of the GSM as an indicator of increased risk of stroke (Biasi et al. 2004; Froio and Biasi 2007; Reiter et al. 2006). Furthermore, GSM can vary between different ultrasound machine manufacturers or between different users depending on the ultrasound machine settings. Plaque characterization by scatter size and attenuation coefficient has been attempted, but no *in vivo* studies have been conducted (Shi et al. 2008b). Thermal strain imaging has been used *in vivo* to detect lipids in atherosclerotic plaques in the femoral arteries of rabbits (Mahmoud et al. 2013). Vulnerable carotid plaque has also been detected using contrast-enhanced ultrasound imaging in combination with tissue Doppler imaging (Deyama et al. 2013), but tissue Doppler imaging has been found to be of limited use because of high variability (Ramnarine et al. 2003).

Two new ultrasound-based elastography methods that have been used to characterize plaque are acoustic radiation force impulse (ARFI) imaging (Allen et al. 2011; Dahl et al. 2009) and shear wave elastography (SWE) (Ramnarine et al. 2014; Widman et al. 2012). Acoustic radiation force impulse imaging can readily distinguish between stiff and soft tissue regions, but can only detect relative stiffness differences between the plaque and the nearby surrounding tissue. SWE still needs to be adapted for plaque measurements, as current results have neglected the viscoelasticity of the carotid artery as well as the shear wave phase aberration effects caused by the cylindrical geometry of the vessel.

Atherosclerotic plaque strain is another measure that has been suggested for detection of plaques liable to rupture. Ultrasound-based speckle tracking is a block-matching technique that estimates strain by tracking interference patterns across imaging frames. Ultrasound speckle tracking plaque characterization has been found feasible with intravascular ultrasound (IVUS) (de Korte et al. 2002; Le Floc'h et al. 2012; Schaar et al. 2003). Moreover, there have been attempts to assess plaque strain non-invasively by radiofrequency-based ultrasound speckle tracking (McCormick et al. 2012; Schmitt et al. 2007).

The driving forces of arterial strain are thought to vary with the type of strain. Radial strain and circumfer-

ential strain are caused by the blood pressure wave during the cardiac cycle. Given conservation of wall volume, radial strain will have a waveform inverse to the pressure wave and be of similar shape. Longitudinal strain is more complex and thought to be caused by a combination of the pressure wave and conservation of volume, wall shear stress from the blood and tethering of the vessel caused by the contracting heart (Cinthio et al. 2006; Hodis and Zamir 2009).

Even though several plaque characterization techniques have been proposed, non-invasive techniques with extensive validation by independent reference methods are, to the best of our knowledge, still lacking. Of the clinically available imaging modalities, it is advantageous to use B-mode ultrasound to characterize plaque because of its low cost, accessibility and tolerability. Recently, our research group published a speckle tracking algorithm based on block matching that successfully estimated strain in the wall of a carotid artery *in silico* (Larsson et al. 2011a), *in vitro* (Larsson et al. 2011b) and validated *in vivo* in a sheep model (Larsson et al. 2013). The aim of this study was to use this speckle tracking algorithm to validate radial and longitudinal strain assessment in plaques by comparing the speckle tracking measurements with sonomicrometry in tissue-mimicking phantoms. Additionally, this study attempted to preliminarily illustrate the feasibility of *in vivo* plaque strain measurements in patients with atherosclerotic plaques, with the hypothesis that soft vulnerable plaques with a large lipid or intraplaque hemorrhage core should exhibit larger strain compared with more stable fibrous plaques.

METHODS

The in-house strain estimation algorithm was first tested in a phantom setup mimicking the carotid artery and validated with sonomicrometry to ensure the accuracy of the algorithm. Upon validation, *in vivo* ultrasound cine loops were collected for patients with carotid *atherosclerotic* plaques in which the strain was calculated.

In vitro experiments

Vessel phantom construction. Four *in vitro* carotid artery phantoms with a plaque-mimicking inclusion were constructed from a mixture (w/w) of 87% de-ionized water, 10% polyvinyl alcohol (PVA) with a molecular weight of 56.140 g/mol (Sigma-Aldrich, St. Louis, MO, USA) and 3% graphite powder with a particle size $<50 \mu\text{m}$ (Merck, Darmstadt, Germany). The solution was heated and stirred until the mixture thickened and was fully dissolved. It was subsequently poured into the vessel phantom mold (Fig. 1a), which consisted of a hollow acrylic block (cylindrical with a 12-mm diameter, 100-mm length

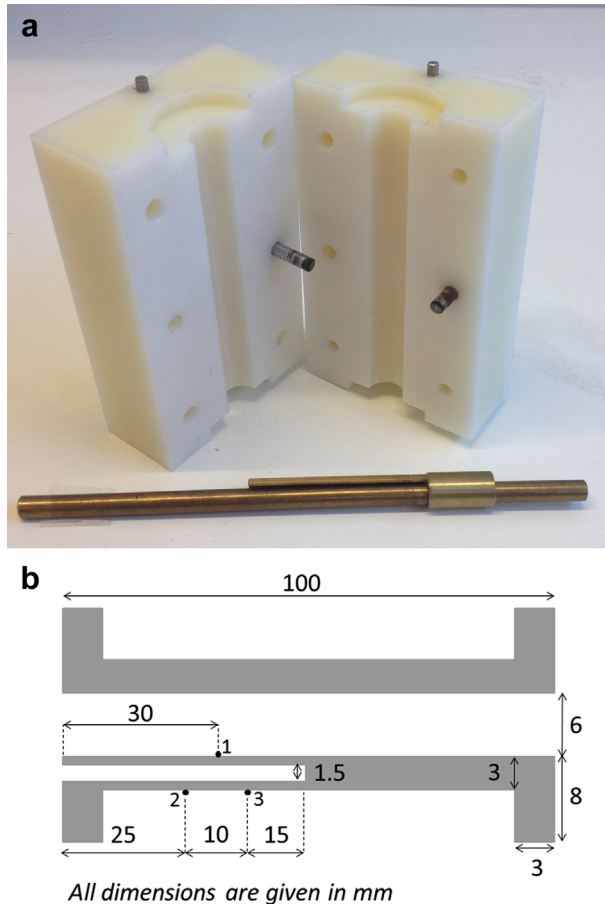


Fig. 1. (a) Acrylic block mold with bronze rod with extension used to create plaque cavity. (b) Long-axis cross-sectional schematic illustration of the phantom with dimensions and placement of sonomicrometry crystals (1–3). Vessel dimensions: 100-mm length, 6-mm lumen diameter, 3-mm wall thickness.

and molded fixing collars) and a 6-mm-diameter bronze rod placed in the center of the hole. The metallic rod had a 50-mm-long, 1.5-mm-thick extension attached to create a cavity in the phantom wall (Fig. 1b).

Once the solution was poured into the mold, it remained confined between the acrylic block and the rod, resulting in a tube-shaped phantom. The phantom was frozen for 12 h at approximately -23°C and then thawed for 12 h at room temperature ($\approx 20^{\circ}\text{C}$). This freeze–thaw cycle was repeated twice for three phantoms and three times for one phantom. Subsequently, the phantom wall cavity was filled with a PVA–graphite solution, prepared as described above, and the entire phantom was exposed to one extra freeze–thaw cycle, resulting in three and four freeze–thaw cycles for the vessel wall and one for the cavity mimicking the plaque. Because PVA stiffens with increasing freeze–thaw cycles, the phantom wall became stiffer than the inclusion, mimicking the vessel wall and the soft plaque, respectively. A photograph of the acrylic

mold and rod and a schematic of the vessel phantom are provided in Figure 1. As the plaque cavity was filled with PVA, the thin vessel wall (0.75 mm) extruded into the lumen, creating a partial lumen occlusion illustrated in Figure 2b.

Experimental setup. The PVA phantoms were attached to a polyvinyl chloride (PVC) box ($100 \times 85 \times 300$ mm) by placing two plastic disks around the fixing collars of the phantoms and tightening them to the fixture with screws (Fig. 2a). The phantoms were aligned in the fixture with the plaque positioned in the posterior wall. To simulate the tissue surrounding the carotid artery, a mixture (w/w) consisting of 3% agar (Merck), 4% graphite powder and 93% de-ionized water by mass was heated 73°C with continuous stirring, then cooled to 40°C and subsequently poured into the PVC box until the PVA–vessel phantom was covered with approximately 1 cm of agar mixture.

The phantoms were connected to a programmable pump (CompuFlow 1000 MR, Shelley Medical Imaging Technologies, London, ON, Canada) by attaching 6-mm-inner-diameter hoses to plastic disks that attached the phantom to the PVC box by compression. The pump was programmed to simulate a carotid flow profile at the rate of 60 cycles/min. A blood-mimicking solution of 40% glycerin (Merck) and 60% de-ionized water mixture was pumped through the phantom at peak flow rates 10, 20, 30 and 35 mL/s. The pump was purged before the experiments to remove air bubbles from the solution.

Data acquisition. Sonomicrometry data and ultrasound cine loops of the plaque and the vessel wall were collected at each flow rate, as illustrated in Figure 3, for each of the four phantoms. Sonomicrometry data were collected for 30 s as a reference strain using a digital sonomicrometry (Sonometrics, London, ON, Canada) acquisition system sampling at 200 Hz. Sonomicrometry crystals 1 mm in diameter were superglued (Loctite, Düsseldorf, Germany) to the plaque lumen and posterior phantom wall (Fig. 1b). The lumen crystal was placed on the cross-sectional apex of the bulging plaque such that it did not touch surrounding vessel walls while simultaneously positioned in-plane with the external crystals. Ultrasound image acquisition was turned off during sonomicrometry data collection to avoid interference between the systems.

Ultrasound long-axis B-mode images were collected on a Vivid E9 ultrasound machine (GE, Horten, Norway) with a fixed 9 LD linear array transducer. Long-axis cine loops were recorded throughout three cycles for each flow rate at a frame rate of 42 Hz, center frequency of 10 MHz and 3.5-cm depth, with one focal point on each phantom wall and image compounding turned off. The imaging plane was positioned close to the plane of the

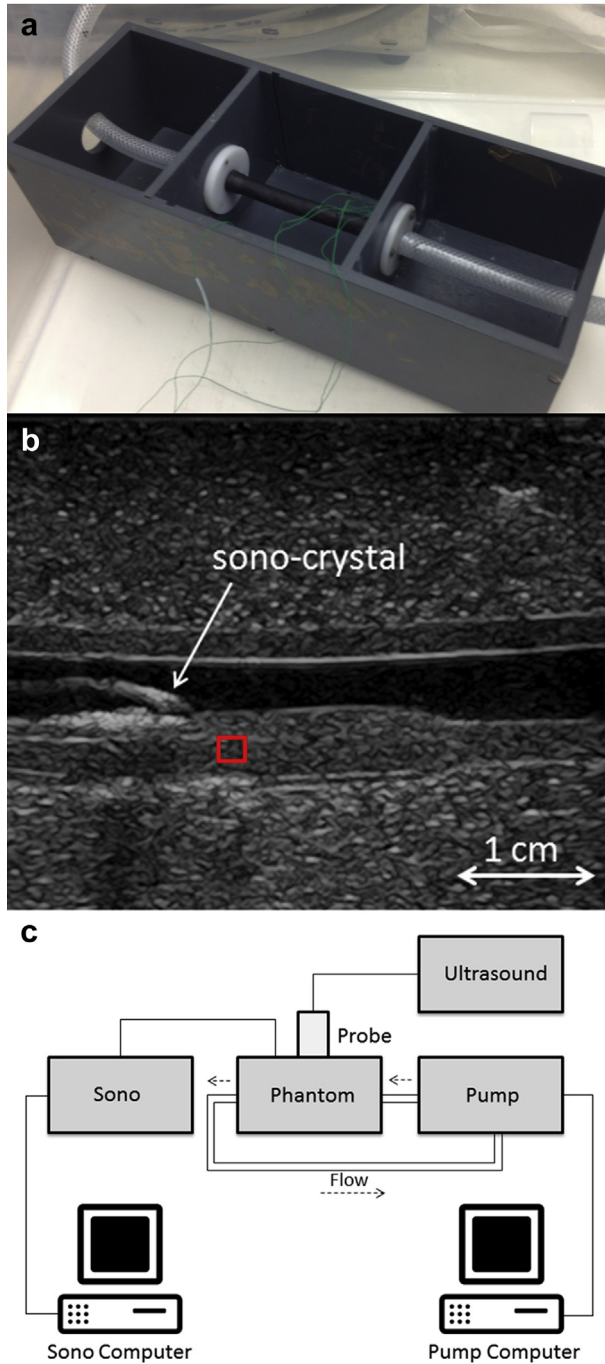


Fig. 2. (a) Photograph of the vessel phantom attached to the polyvinyl chloride box connected to the pump before the cavity was filled with the agar mixture. The wires are leads to the sonomicrometry crystals. (b) B-mode long-axis image of the phantom vessel with a soft plaque inclusion to the left in the posterior wall. The red box indicates the region of interest for the speckle tracking radial strain analysis offset to the right of the lumen sono-crystal to avoid the shadowed region. (c) Diagram of the experimental setup illustrating connections between the phantom, sonomicrometry system, programmable pump and ultrasound machine.

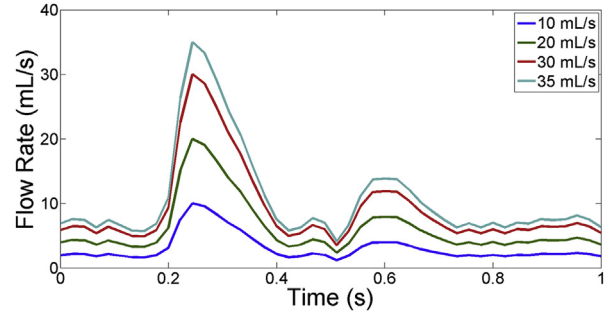


Fig. 3. CompuFlow 1000 MR programmable pump (Shelley Medical Imaging Technologies, London, ON, Canada) carotid artery flow profile curves for 10, 20, 30 and 35 mL/s.

sonomicrometry crystals, making them visible. Figure 2b is a sample B-mode long-axis image of the phantom with plaque inclusion embedded in the agar mixture. A schematic of the experimental setup is provided in Figure 2c.

Data analysis. The collected sonomicrometry and B-mode data were analyzed in MATLAB 2011a (The MathWorks, Natick, MA, USA) and synchronized by recording a simulated electrocardiogram signal from the CompuFlow 1000 MR pump. A speckle tracking algorithm developed in-house was used to calculate the peak plaque strain, which was compared with the strain found from the movement recorded by the sonomicrometry crystals.

Speckle tracking analysis. The in-house speckle tracking algorithm (Larsson et al. 2011a) based on normalized cross-correlation was used to perform the speckle tracking analysis. Axial (along the ultrasound beam) and lateral (orthogonal to the ultrasound beam) motion estimation was performed on three consecutive pump cycles on the envelope-detected signal with kernel length and width of 3 and 5 wavelengths (λ), respectively. The kernel size was selected based on previous successful experiments measuring strain in the carotid wall both *in vitro* (Larsson et al. 2011b) and *in vivo* (Larsson et al. 2013). The kernel was moved in a search area that was defined to allow maximum velocities of 2 cm/s with 60% axial and lateral overlap using spline interpolation to detect subsample motion. Accumulation of the displacement maps throughout the cardiac cycle was then performed using linear interpolation to account for subpixel motion to assess the cumulative strain. The radial (along the vessel radius) and longitudinal (along the vessel axis) speckle tracking strain curves were then obtained by linear regression in a region of interest (ROI) and subsequently low pass filtered with an averaging window three samples in length to remove noise. All parameters described were chosen based on a

previous study in a carotid artery phantom wall (Larsson *et al.* 2011b) and then modified to optimize the algorithm for measuring strain in plaques.

For plaque strain estimation, the ROI size was based on diastolic measurements of the size of the plaque. The ROI was manually selected near the vertical center of the plaque, offset to the right of the sonomicrometry crystal in the lumen to avoid effects of shadowing. The ROI for radial strain was selected to be approximately 50% of the plaque height and 1.5 mm in width. The longitudinal ROI width was approximately 50% of the distance from the crystal to the apex of the plaque (typically 4 mm wide) and 1.5 mm in height.

For vessel wall strain estimation, two of the phantoms were used for comparison between vessel wall and plaque strain. The vessel wall ROI was placed on the same posterior side of the phantom as the plaque to achieve similar boundary conditions from the PVC box and agar mixture. The ROI was manually placed approximately 2 cm from the plaque in the center of the vessel wall with a ROI widths and heights of 1.5×1.5 and 5×1.5 mm in the radial and longitudinal directions, respectively.

Sonomicrometry analysis. Outliers from the inter-crystal displacement curves were removed by thresholding, followed by filtering of the resulting signals with a median filter 10 samples in length. Five cycles were averaged to obtain the final reference displacement curves. Because the crystals were positioned in a triangle, the law of cosines was used to calculate the radial displacement, whereas the longitudinal displacement was the distance between crystals 2 and 3 (Fig. 1b). Thus, the strain, $\varepsilon(t)$, was calculated as

$$\varepsilon(t) = \frac{D(t) - D_0}{D_0} \quad (1)$$

where D_0 is the initial distance between the crystals, and $D(t)$ is the distance between the crystals at time t .

Speckle tracking sonomicrometry comparison. The root mean square error (RMSE) was calculated on the first cycle of B-mode data for each flow condition per phantom as

$$\text{RMSE} = \sqrt{\frac{\sum_{n=1}^N (\varepsilon(n) - \hat{\varepsilon}(n))^2}{N}} \quad (2)$$

where $\varepsilon(n)$ is the reference sonomicrometry strain, $\hat{\varepsilon}(n)$ is the estimated speckle tracking strain and N is the number of frames in one pump cycle. Absolute peak error was calculated as the absolute difference between the reference and estimated peak systolic strain ($|\varepsilon_{\text{peak}} - \hat{\varepsilon}_{\text{peak}}|$) and averaged for all flow conditions and phantoms.

Bland–Altman plots for sonomicrometry and speckle tracking peak strain were created, and correlation analysis was performed. A paired t -test was performed to compare plaque and wall peak strain.

In vivo experiments

Data acquisition. Long-axis and short-axis ultrasound cine loops were collected from seven patients (mean age: 77 ± 6 y, 4 males, 3 females) on a GE Vivid E9 ultrasound machine (Horten, Norway) with a hand-held 9 LD linear array transducer by an experienced ultrasound technician. The images were acquired with a center frequency of 10 MHz, 3.5-cm depth, with two focal points on the arterial walls and image compounding turned off at a frame rate of 42 Hz, similar to the *in vitro* setup. The procedure consisted of collecting three long-axis and short-axis cine loops over three consecutive cardiac cycles for the common carotid artery, the bulb and the internal carotid artery. Patient medical data including sex, age and blood pressure were collected at Karolinska University Hospital, Huddinge, Sweden, with consent given by the patients and approval by the ethical review board.

Data analysis. Plaque classification. Before speckle tracking analysis, the cine loops from the patients were visually analyzed and scored by two experienced physiologists. If a plaque was present and of sufficient size (diameter > 2 mm), the physicians outlined the borders in diastole, which later served as boundaries for ROI placement during speckle tracking analysis. The cine loops were scored using four different measures. First, the plaque was classified as homogeneous or heterogeneous. Homogeneous plaques have a uniform texture and contain uniform echoes with medium-to high-level intensity compared with the nearby adventitia. Heterogeneous plaques have mixed-level echoes and contain one or more echolucent areas (low-level echoes). Plaque echogenicity was compared with echogenicity of blood and adjacent adventitia. Low-level echoes were defined as those approaching echo levels of blood, and medium-to high-level echoes were defined as echo strength similar or greater than that of adventitia or adjacent soft tissue. Second, the plaque was classified as to whether its surface was smooth or irregular based on visual interpretation of gray-scale and color Doppler images (Fitzgerald and O'Farrell 1993; Kanber *et al.* 2013b).

The third method was to subjectively classify the plaque on a Gray-Weale four-level scale: type 1 = mainly echolucent lesions, type 2 = primarily echolucent lesions with some areas of echogenicity, type 3 = dominantly echogenic, type 4 = uniformly echogenic. Types 1 and 2 correspond to heterogeneous plaques, and types 3 and 4

correspond to homogeneous plaques, which consist mainly of fibrous tissue (Bluth 1997).

Fourth, the GSM of the plaque was measured using Automated Measurement System (AMS), which was developed by the Department of Signals and Systems at Chalmers University of Technology, Gothenburg, Sweden, and the Physiology Group at the Wallenberg laboratory, Gothenburg University, Gothenburg, Sweden. The GSM was measured on a single frame of the cine loop in systole and used as an alternative measurement of echogenicity. The image was normalized by semi-automatically selecting the brightest and darkest pixels in the image and then calculating the GSM from image analyses of the physician-outlined plaque, returning a median pixel value in the range 0 (black) to 255 (white).

Speckle tracking analysis. After plaque scoring, the cine loops were analyzed with the in-house speckle tracking algorithm with similar parameters as in the phantom setup. If the plaque diameter was <2 mm, the kernel size was reduced to a width and length of 2λ and 4λ , respectively, to allow for a smaller ROI. The ROI varied with plaque size and shape, was made as large as possible without exceeding the outlined plaque borders and was manually placed in the center of the plaque as identified by the physiologists. The speckle tracking strain curves

were low pass filtered with a uniform averaging window three samples in length to remove noise. Plaque strain was estimated in all three carotid artery locations given that plaque was present and was of adequate size (diameter > 1.5 mm) and that the image was of sufficient quality. Peak negative radial strain and peak positive longitudinal strain in the plaque from two cardiac cycles were calculated and averaged for each plaque. Thereafter, the radial and longitudinal peak strains were adjusted for the patients' pulse pressure (the difference between systolic and diastolic blood pressures). Pulse pressure-adjusted peak negative radial and positive longitudinal strains, GSM and GSM variance (variance of pixel values within the plaque) were compared between plaques scored on the Gray-Weale scale.

RESULTS

In vitro

Sample speckle tracking and sonomicrometry plaque strain curves for radial and longitudinal strain are provided in Figure 4a and Figure 4c, respectively. In Figure 4(b, d) are the correlation plots of speckle tracking versus sonomicrometry for radial ($r = 0.96$, $p < 0.001$) and longitudinal ($r = 0.75$, $p \leq 0.01$) peak strains, respectively. The radial and longitudinal Bland-Altman plots

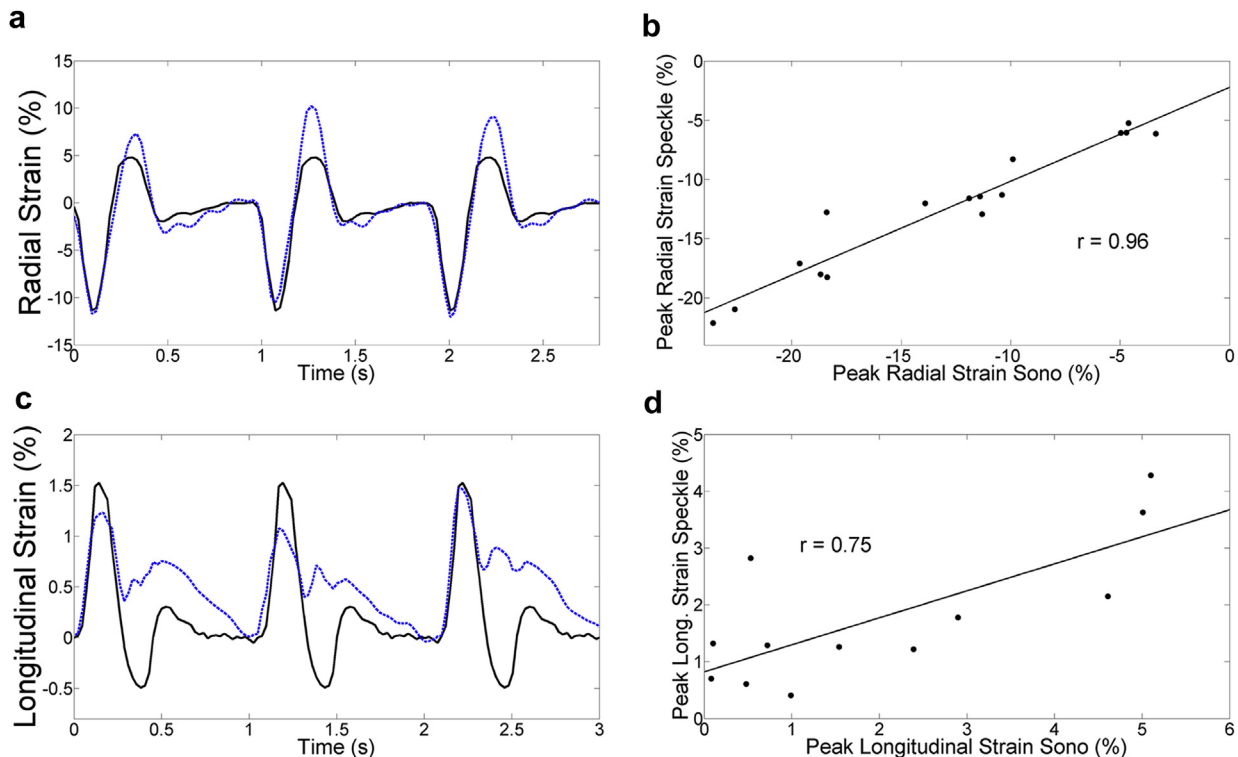


Fig. 4. Sample *in vitro* plaque strain curves for sonomicrometry (solid line) and speckle tracking (blue dashed line) for the radial (a) and longitudinal (c) directions. Correlation plots for negative radial (b) and positive longitudinal (d) peak speckle tracking strain versus peak sonomicrometry strain, along with correlation values.

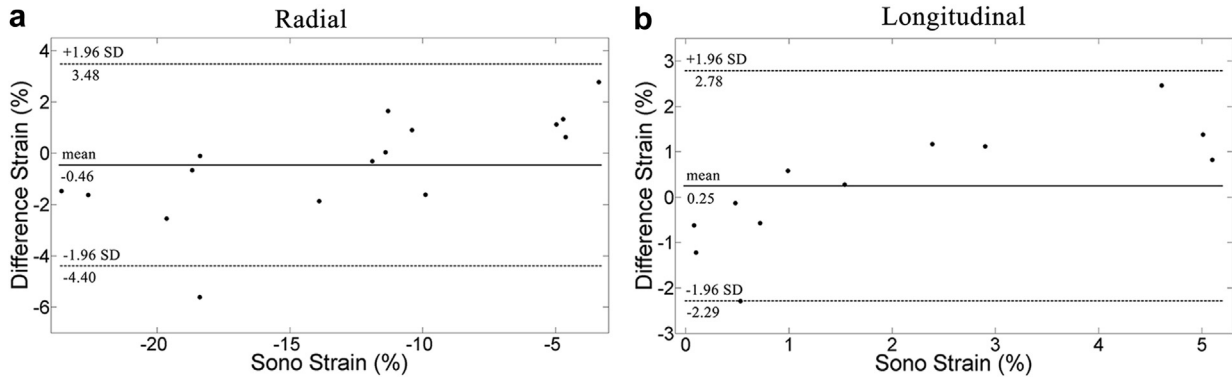


Fig. 5. Radial (a) and longitudinal (b) Bland–Altman plots of difference between sonomicrometry strain and speckle tracking strain versus sonomicrometry strain.

are provided in Figure 5a and Figure 5b, respectively. Radial and longitudinal limits of agreement (LOA) were -4.40% to 3.48% and -2.29% to 2.78% , respectively. Table 1 lists the means and standard deviations for the absolute peak error and RMSE for the radial and longitudinal strains. Longitudinal strain data were discarded for one of the phantoms because of irregular movement caused by fluid in the plaque cavity. The plaque exhibited $35.1 \pm 16.9\%$ greater radial ($p < 0.001$) and $88.6 \pm 72.0\%$ greater longitudinal ($p < 0.001$) peak strain compared with the arterial wall when measured with speckle tracking.

In vivo

Sixteen plaques were present in the patient population from which seven data points were removed because of poor image quality or too small plaque size ($n = 9$). Figure 6 illustrates the pulse pressure-adjusted means of peak strains and standard deviations for plaques in the radial (a) and longitudinal (b) directions sorted by Gray-Weale classification. The mean peak strain values and standard deviations for radial and longitudinal plaque strain, as well as the pulse-pressure adjusted values, are listed in Table 2 sorted by Gray-Weale classification.

Table 3 summarizes plaque locations and classification results. Sample echogenic and echolucent plaques can be seen in Figure 7a and Figure 7d, respectively, with a physician-outlined border (green line) and ROI (red rectangle). Also in Figure 7 are *in vivo* sample

Table 1. *In vitro* strain estimation results from speckle tracking analysis in plaques

	Radial strain	Longitudinal strain
Absolute peak error (%)	$2.09 \pm 2.03^*$	1.61 ± 1.57
Root mean square error (%)	2.93 ± 2.18	0.78 ± 0.49

* Mean \pm standard deviation.

speckle tracking strain curves in the radial (b, e) and longitudinal (c, f) directions for the echogenic and echolucent plaques, respectively.

The measured mean and standard deviation plaque GSMs by Gray-Weale classification were (type 1) 40 ± 0 , (type 2) 84 ± 9 and (type 3) 53. In Figure 8, GSM variance in the plaque is plotted versus Gray-Weale classification.

DISCUSSION

Non-invasive characterization of carotid artery plaque based on quantitative data would be a valuable tool for physicians to determine treatment options for patients with atherosclerosis. Current standards limit physicians to visual assessment of ultrasound B-mode images and carotid angiograms, allowing observer error to influence the results (Arnold *et al.* 1999). The goal of this study was to validate an in-house speckle tracking algorithm based on block matching to quantify the strain of the plaque in a phantom setup with sonomicrometry and to perform a small pilot study *in vivo*. To the best of our knowledge, assessment of plaque strain in ultrasound carotid images has not been validated with an independent method.

In vitro study

The validation study indicates good agreement between the speckle tracking algorithm and sonomicrometry. A strong correlation between speckle tracking and reference strain values was found radially (Fig. 4b); agreement in the longitudinal direction (Fig. 4d) was not as strong, but still good. This was most likely due to the intrinsic lower resolution in the lateral direction coupled with little longitudinal plaque movement. The radial and longitudinal absolute peak error and RMSE (Table 1) indicate less absolute error in the longitudinal strain. However, it must be taken into consideration that

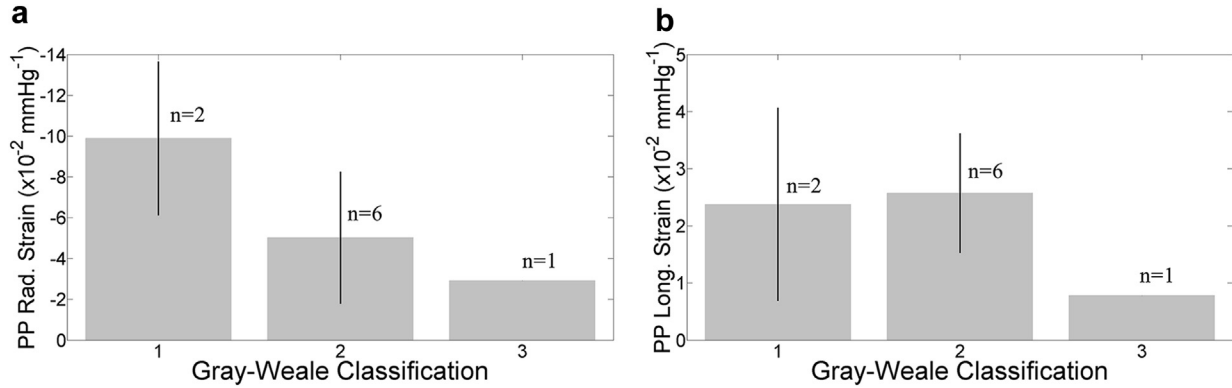


Fig. 6. Pulse pressure (PP)-adjusted means and standard deviations for radial (a) and longitudinal (b) strains for *in vivo* plaques sorted by Gray-Weale classification.

radial strain is significantly larger in magnitude than longitudinal strain. The radial and longitudinal Bland–Altman plots (Fig. 5) indicate that the speckle tracking algorithm overestimates low strain values and underestimates high strain values. Radially, the LOA are acceptable in relation to the range, whereas the longitudinal LOA are higher as a result of two outliers (Fig. 5b). Nevertheless, there is still good correlation ($r = 0.75$) between sonomicrometry and speckle tracking in the longitudinal direction.

Creating a phantom with a soft plaque inclusion was challenging, resulting in several design modifications. Eight phantoms were attempted, only four of which succeeded. The first two successful phantoms leaked fluid into the plaque cavity when connected to the pump. This resulted in less radial and longitudinal plaque strain combined with longitudinal plaque compression in one of the phantoms. Furthermore, the fluid degraded the image quality of the plaque. The final two phantoms were modified by supergluing the plaque cavity shut after the final freeze cycle to prevent fluid in the lumen from leaking into the cavity. These phantoms were used for the strain comparison between plaque and vessel wall.

A second source of error was the placement of the lumen sonomicrometry crystal on the plaque (Fig. 1b, crystal 1). Limited visibility and accessibility made it difficult to place the crystal on the center of the lumen plaque extrusion. Off-center placement can result in un-

derestimation of radial displacement. The fairness of comparing sonomicrometry and speckle tracking could also be questioned, because the crystals and ROIs were not placed at the exact same location in the plaque to avoid the shadowed region under the crystals (Fig. 2b).

During the cardiac cycle, the radial strain in the phantom plaque had a significant gradient as a result of greater plaque movement near the lumen in contrast to the plaque boundary facing the posterior wall. To avoid these extremes, the ROI was placed in the center of the plaque and the ROI height was limited to 50% of the vertical plaque size to measure an average value for the plaque strain. The strain gradient was not significant in the *in vivo* experiment as it is an effect of the experimental setup from the boundary conditions imposed on the phantom by the agar mixture and glycerin blood-mimicking fluid. It should be mentioned that moving the kernel in a search area defined to allow maximum velocities of 2 cm/s can be a potential tracking limitation of the speckle tracking algorithm; however, this was not experienced as a limitation *in vivo* or *in vitro*. Additionally, the algorithm does not take into account out-of-plane motion. In other strain studies involving carotid artery-mimicking phantoms, the vessel was placed in a water bath while the intraluminal pressure was varied statically (Ribbers et al. 2007). Initial pilot tests indicated that the flow profiles from the pump induced a ringing artifact in the phantom at the end of the cardiac cycle when surrounded by water

Table 2. *In vivo* strain estimation results from speckle tracking analysis in plaques sorted by Gray-Weale classification

Gray-Weale classification	Radial strain (%)	PP-adjusted radial strain ($\times 10^{-2} \text{ mm Hg}^{-1}$)	Longitudinal strain (%)	PP-adjusted longitudinal strain* ($\times 10^{-2} \text{ mm Hg}^{-1}$)
1	$-5.4 \pm 1.5^*$	-9.9 ± 2.7	1.3 ± 0.7	2.4 ± 1.2
2	-2.7 ± 1.4	-5.0 ± 2.9	1.3 ± 0.5	2.1 ± 1.0
3	-2.6	-2.9	0.7	0.8

PP = pulse pressure.

* Mean \pm standard deviation.

Table 3. *In vivo* plaque location and classification results

Plaque no.	Location	Consistency	Smooth vs. rough surface	Visual classification	Gray-Weale score (1–4)
1	Bulb	Heterogeneous	Rough	DL	2
2	ICA	Heterogeneous	Rough	DL	2
3	CCA	Heterogeneous	Smooth	DL	2
4	ICA	Heterogeneous	Rough	DL	2
5	CCA	Heterogeneous	Rough	DL	2
6	Bulb	Homogeneous	Rough	DL	2
7	Bulb	Heterogeneous	Rough	DG	3
8	Bulb	Homogeneous	Smooth	L	1
9	ICA	Homogeneous	Smooth	L	1

Bulb = carotid artery bulb; CCA = common carotid artery; ICA = internal carotid artery; L = echolucent; DL = dominant echolucent; DG = dominant echogenic; G = echogenic.

in the fixture. By mimicking the boundary conditions imposed by the surrounding tissue with the agar mixture, the ringing was damped and the axial motion in the phantom was similar to that of the programmed flow profile. It should also be noted that in this experimental setup, a plaque in the common carotid artery was mimicked, but it is

more common for plaque buildup to occur in the artery bifurcation (Oviedo *et al.* 2010).

Despite these limitations, the two methods are in good agreement, and it is possible to distinguish the plaque from the arterial wall. These results are in line with other studies indicating that it is feasible to measure

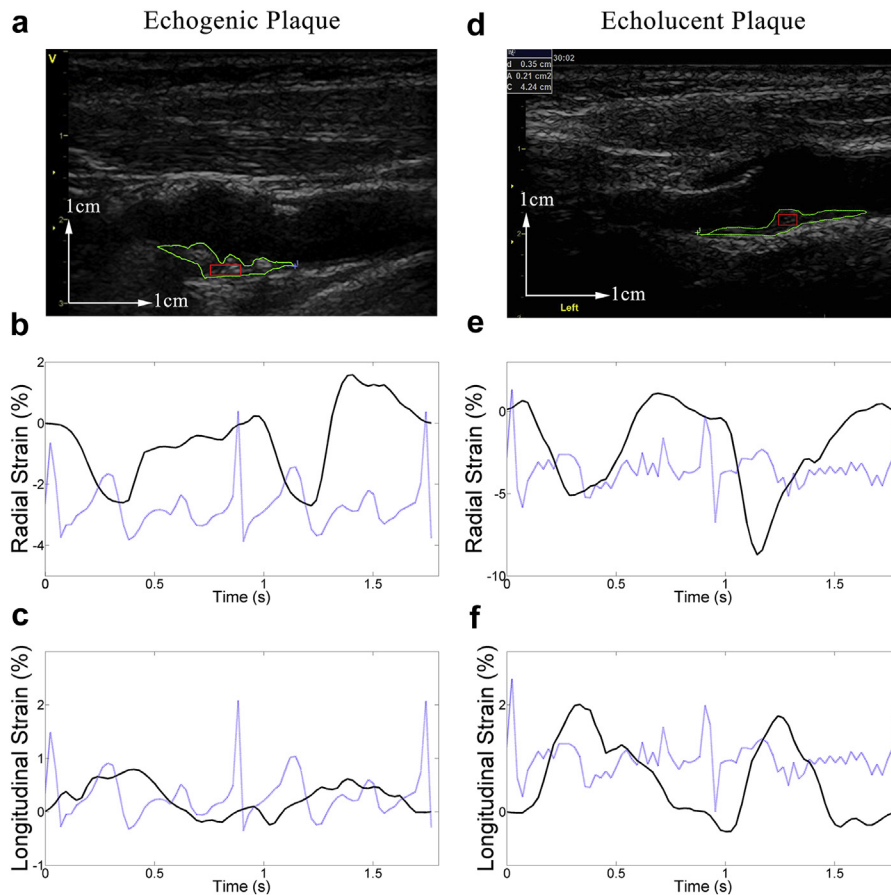


Fig. 7. *In vivo* B-mode ultrasound images for an (a) echogenic plaque located in the right internal carotid artery of a 72-year-old woman and an (d) echolucent plaque located in the left carotid artery bulb of a 78-year-old man. The green line is the physicians' outline of the plaques; the regions of interest for speckle tracking analysis are in red. (b, c, e, f) Strain curves (black) for radial (b, e) and longitudinal (c, f) directions for echogenic (left column) and echolucent (right column) plaques, respectively. The patient's electrocardiogram curves are displayed as blue dotted curves in (b), (c), (e) and (f).

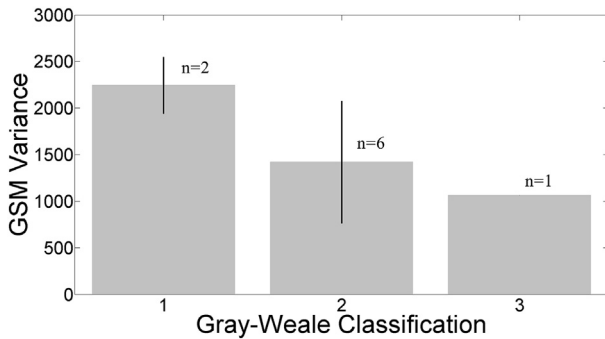


Fig. 8. Gray-scale median (GSM) variance versus Gray-Weale classification for *in vivo* plaques.

plaque strain *in vivo* (de Korte et al. 2002; Golemati et al. 2012; Le Floc'h et al. 2012; McCormick et al. 2012; Schmitt et al. 2007). In addition, Schaar et al. (2003) obtained high sensitivity (88%) and specificity (89%) when characterizing plaque with strain using IVUS. Other techniques have used accumulated axial strain and relative lateral shifts as intricacies for plaque strains using IVUS with positive results (Shi et al. 2008a), yet these techniques are invasive.

In vivo study

The *in vivo* study illustrates that it is possible to estimate plaque strain by speckle tracking *in vivo* using B-mode ultrasound. The results indicate an increase in radial strain for mainly echolucent plaques in contrast to dominantly echogenic plaques (Fig. 6a). This is in agreement with our hypothesis that the force from the blood of the cardiac systolic pressure wave induces greater deformation in echolucent plaques with a large lipid or intra-plaque hemorrhage core, in contrast to echogenic plaques composed of relatively homogeneous fibrous tissue. Gray-Weale type 1 and 2 plaques exhibited increased longitudinal strain compared with the type 3 plaque (Fig. 6b). Both radial and longitudinal strain results were normalized to the patient's pulse pressure because it is the driving force for radial strain and one of the forces, in addition to shear forces from blood flow and tethering forces from the heart, for longitudinal strain. Without normalization, variation in blood pressure between patients could bias the results.

Sample strain curves illustrate increased radial (Fig. 7b, e) and longitudinal (Fig. 7c, f) strain for an echolucent plaque (Fig. 7d) compared with an echogenic plaque (Fig. 7a). The strain curves also indicate the reproducibility over two cardiac cycles given that the ultrasound cine loop is of good quality. Reproducibility requires the transducer and patient to be motionless for approximately 3 s during image acquisition. In practice, this is quite difficult for elderly patients, especially those with additional ailments and illnesses. Given the small arterial motions

and strains, stabilization of the ultrasound probe in a fixture would be essential in clinical applications and could potentially improve results and reproducibility. Furthermore, the plaque must be of sufficient size (diameter > 1.5 mm) to achieve reliable measurements. These two constraints limited us from successfully measuring strain in all *in vivo* plaque data. The *in vivo* waveforms (Fig. 7b, c, e, f) vary more from cycle to cycle compared with the *in vitro* waveforms in Figure 4(a, c). This can be explained by the fact that the *in vitro* phantoms are connected to a pump controlled by a precision stepper motor with images acquired from a stationary transducer, whereas the *in vivo* arterial wall motion is driven by a variable heart rate and stroke volume with image acquisition influenced by patient and transducer motion. The *in vivo* longitudinal strains (Fig. 7c, f) are also influenced by different shear forces than the *in vitro* phantom vessel because of more complex arterial wall and plaque surface composition, as well as differences in fluid properties between blood and the blood-mimicking glycerin mixture used in the phantom, which also could contribute to the more complex *in vivo* strain waveforms. Moreover, *in vitro* longitudinal strain does not experience any of the tethering forces from the pumping of the heart, which influences longitudinal *in vivo* strain.

De Korte et al. (2002) investigated the identification of atherosclerotic plaque components in external iliac and femoral arteries using IVUS elastography in an *in vivo* Yucatan pig study. Peak radial strain values up to 2% for echolucent plaques were recorded, which is slightly less than our absolute peak radial strain values (4%–7%) for echolucent plaques. Different arterial locations and pressures, as well as different species, may explain the difference in measured strain.

Sztajzel et al. (2005) and Salem et al. (2012) found that plaques with large calcifications had the highest GSM values, fibrous plaques had intermediate GSM values and those with large hemorrhagic areas or with a predominant necrotic core exhibited the lowest. Nevertheless, in our limited data set, no relationship was found between GSM and plaque echogenicity, which could be attributed to measuring the GSM on a single frame rather than averaging the GSM throughout the cardiac cycle. However, Figure 8 illustrates that GSM variance was greater for echolucent plaques than for echogenic plaques. The reliability of GSM as a quantitative tool for measuring plaque vulnerability has been disputed. GSM is an overall measure of plaque echogenicity, making it possible for a plaque to have average GSM values even with highly echolucent areas because of counterbalancing echogenic areas. In contrast to previous studies (Sabetai et al. 2000), Kolkert et al. (2014) recently reported that there is no additional value to the use of GSM in evaluating plaque vulnerability.

Some study limitations deserve to be pointed out. Generally, classifying atherosclerotic plaques as “hard” or “soft” is most likely an oversimplification. From our small sample population we found that the majority of plaques are a mixture of echogenic and echolucent regions, making them very difficult to classify on the Gray-Weale scale, allowing for subjectivity in the interpretation. In addition, it is very difficult to classify plaques strictly on long-axis B-mode images, as clinicians are accustomed to using long-axis and short-axis images, as well as Doppler color flow (Arnold *et al.* 1999). Certain plaque–lumen borders were not clearly defined, making it difficult for the physicians to outline the plaque, as well as assess the plaque surface. Qualitative assessment of plaque surface irregularities is subjective, but more quantitative methods are being developed (Kanber *et al.* 2013b). A larger and more variable sample population would have been desirable with several plaques in all Gray-Weale scale categories. We acknowledge that the study is limited by the presence of only one type 3 dominantly echogenic plaque. However, we emphasize that these are preliminary results and we plan to conduct a larger clinical study in the future.

Measuring strain in plaques with a mixture of echolucent and echogenic regions can be difficult. In complex plaque geometries with mixed regions, such as in Figure 7(a), it is not intuitive where to place the rectangular ROI. We attempted to place the ROI in both echolucent and echogenic regions of the plaque to get an average strain value for the motion in both regions.

Alternative motion tracking methods could potentially improve plaque tracking in future studies. Golemati *et al.* (2012) compared block matching and differential methods for motion analysis of the carotid artery wall. Four techniques were compared: optical flow; weighted least-squares optical flow; block matching; and affine block motion model. It was found that least-squares optical flow performed best on simulated B-mode images. However, the study lacked validation against an independent strain measurement method, such as sonomicrometry.

Future *in vivo* studies should include a larger sample population and a ROI that follows the physician’s plaque outline. A contrast agent could potentially improve the edge detection of the plaques, resulting in improved motion tracking. To avoid subjective plaque classification, the sample population should consist of patients undergoing an endarterectomy procedure to allow for plaque classification with histology. If a large enough plaque strain database is collected and validated against histology, physicians could potentially use the technique to assess the vulnerability of plaques. Finally, this study did not include circumferential plaque strain, which could be of potential clinical significance.

CONCLUSIONS

This study illustrates the feasibility of radial and longitudinal speckle tracking strain estimation of plaque in the carotid artery, which was validated by sonomicrometry in a plaque phantom. The results indicate the possibility of characterizing plaque vulnerability based on strain, but the algorithm must be applied in a larger study to build a plaque strain database validated against histology. Preliminary results indicate increased radial and longitudinal strain in dominantly echolucent and primarily echolucent plaques with some areas of echogenicity, compared with strain in echogenic plaques.

Acknowledgments—This study was supported by VINNOVA VINNMER Marie Curie International Qualification (grant 2011-01365), the Swedish Heart–Lung Foundation (grant 2012-2795) and the Swedish Research Council (grant 2011-0656). We thank Rita Balzano and Linnea Sandersjö for collecting *in vivo* ultrasound images and Dr. Kent Lund for performing the clinical plaque classification.

REFERENCES

- Allen JD, Ham KL, Dumont DM, Sileshi B, Trahey GE, Dahl JJ. The development and potential of acoustic radiation force impulse (ARFI) imaging for carotid artery plaque characterization. *Vasc Med* 2011;16:302–311.
- Armas R, Kirkwood JR, Zubi S. The posterior cerebral radionuclide angiogram for the detection of carotid artery disease. *Clin Nucl Med* 1981;6:19–22.
- Arnold JA, Modaresi KB, Thomas N, Taylor PR, Padayachee TS. Carotid plaque characterization by duplex scanning: Observer error may undermine current clinical trials. *Stroke* 1999;30:61–65.
- Biasi GM, Froio A, Diethrich EB, Deleo G, Galimberti S, Mingazzini P, Nicolaides AN, Griffin M, Raitheil D, Reid DB, Valsecchi MG. Carotid plaque echolucency increases the risk of stroke in carotid stenting: The Imaging in Carotid Angioplasty and Risk of Stroke (ICAROS) study. *Circulation* 2004;110:756–762.
- Biasi GM, Sampaolo A, Mingazzini P, De Amicis P, El-Barghouty N, Nicolaides AN. Computer analysis of ultrasonic plaque echolucency in identifying high risk carotid bifurcation lesions. *Eur J Vasc Endovasc* 1999;17:476–479.
- Bluth EI. Evaluation and characterization of carotid plaque. *Semin Ultrasound CT MR* 1997;18:57–65.
- Cinthio M, Ahlgren AR, Bergkvist J, Jansson T, Persson HW, Lindstrom K. Longitudinal movements and resulting shear strain of the arterial wall. *Am J Physiol Heart Circ Physiol* 2006;291:H394–H402.
- Dahl JJ, Dumont DM, Allen JD, Miller EM, Trahey GE. Acoustic radiation force impulse imaging for non-invasive characterization of carotid artery atherosclerotic plaques: A feasibility study. *Ultrasound Med Biol* 2009;35:707–716.
- De Korte CL, Sierevogel MJ, Mastik F, Strijder C, Schaar JA, Velema E, Pasterkamp G, Serruys PW, van der Steen AF. Identification of atherosclerotic plaque components with intravascular ultrasound elastography *in vivo*: A Yucatan pig study. *Circulation* 2002;105:1627–1630.
- Deyama J, Nakamura T, Takishima I, Fujioka D, Kawabata K, Obata JE, Watanabe K, Watanabe Y, Saito Y, Mishina H, Kugiyama K. Contrast-enhanced ultrasound imaging of carotid plaque neovascularization is useful for identifying high-risk patients with coronary artery disease. *Circ J* 2013;77:1499–1507.
- Easton JD, Wilterdink JL. Carotid endarterectomy: Trials and tribulations. *Ann Neurol* 1994;35:5–17.
- Fitzgerald DE, O’Farrell CM. Prognostic value of ultrasound morphology in carotid atherosclerosis. *Int Angiol* 1993;12:337–341.

- Froio A, Biasi GM. Carotid plaque echolucency predicts the risk of stroke in carotid stenting according to the type of brain protection device and the learning curve. *Stroke* 2007;38:e67. author reply e8.
- Golemati S, Stoitsis JS, Gastounioli A, Dimopoulos AC, Koropouli V, Nikita KS. Comparison of block matching and differential methods for motion analysis of the carotid artery wall from ultrasound images. *IEEE Trans Inf Technol Biomed* 2012;16:852–858.
- Gray-Weale AC, Graham JC, Burnett JR, Byrne K, Lusby RJ. Carotid artery atheroma: Comparison of pre-operative B-mode ultrasound appearance with carotid endarterectomy specimen pathology. *J Cardiovasc Surg (Torino)* 1988;29:676–681.
- Hodis S, Zamir M. Arterial wall tethering as a distant boundary condition. *Phys Rev E* 2009;80:051913.
- Kakkos SK, Griffin MB, Nicolaidis AN, Kyriacou E, Sabetai MM, Tegos T, Makris GC, Thomas DJ, Geroulakos G, Ri ACS. The size of juxtaluminal hypochoic area in ultrasound images of asymptomatic carotid plaques predicts the occurrence of stroke. *J Vasc Surg* 2013;57:609–617.
- Kanber B, Hartshorne TC, Horsfield MA, Naylor AR, Robinson TG, Ramnarine KV. Dynamic variations in the ultrasound gray-scale median of carotid artery plaques. *Cardiovasc Ultrasound* 2013a;11:21.
- Kanber B, Hartshorne TC, Horsfield MA, Naylor AR, Robinson TG, Ramnarine KV. Quantitative assessment of carotid plaque surface irregularities and correlation to cerebrovascular symptoms. *Cardiovasc Ultrasound* 2013b;11:38.
- Kolkert JL, Meerwaldt R, Loonstra J, Schenk M, van der Palen J, van den Dungen JJ, Zeebregts CJ. Relation between B-mode gray-scale median and clinical features of carotid stenosis vulnerability. *Ann Vasc Surg* 2014;28:404–410.
- Larsson M, Kremer F, Claus P, Kuznetsova T, Brodin LA, D'hooge J. Ultrasound-based radial and longitudinal strain estimation of the carotid artery: A feasibility study. *IEEE Trans Ultrason Ferroelectr Freq Control* 2011a;58:2244–2251.
- Larsson M, Kremer F, Heyde B, Brodin LA, D'hooge J. Ultrasound-based speckle tracking for 3-D strain estimation of the arterial wall: An experimental validation study in a tissue mimicking phantom. In: *Proceedings, IEEE International Ultrasonics Symposium, Orlando, Florida, USA, 18–21 October 2011*. New York: IEEE; 2011b. p. 725–728.
- Larsson M, Verbrugge P, Smoljkic M, Heyde B, Famaey N, Herijgers P, D'Hooge J. Assessment of longitudinal strain in the carotid artery wall using ultrasound-based speckle tracking—Validation in a sheep model. In: *Proceedings, IEEE International Ultrasonics Symposium, Prague, Czech Republic, 21–25 July 2013*. New York: IEEE; 2013. p. 569–572.
- Le Floc'h S, Cloutier G, Saijo Y, Finet G, Yazdani SK, Deleaval F, Rioufol G, Pettigrew RI, Ohayon J. A four-criterion selection procedure for atherosclerotic plaque elasticity reconstruction based on *in vivo* coronary intravascular ultrasound radial strain sequences. *Ultrasound Med Biol* 2012;38:2084–2097.
- Mahmoud AM, Dutta D, Lavery L, Stephens DN, Villanueva FS, Kim K. Noninvasive detection of lipids in atherosclerotic plaque using ultrasound thermal strain imaging: *In vivo* animal study. *J Am Coll Cardiol* 2013;62:1804–1809.
- Matos JM, Barshes NR, McCoy S, Pisimisis G, Felkai D, Kougiass P, Lin PH, Bechara CF. Validating common carotid stenosis by duplex ultrasound with carotid angiogram or computed tomography scan. *J Vasc Surg* 2014;59:435–439.
- McCormick M, Varghese T, Wang X, Mitchell C, Kliewer MA, Dempsey RJ. Methods for robust *in vivo* strain estimation in the carotid artery. *Phys Med Biol* 2012;57:7329–7353.
- Mono ML, Karameshev A, Slotboom J, Remonda L, Galimanis A, Jung S, Findling O, De Marchis GM, Luedi R, Kiefer C, Stucker C, Mattle HP, Schroth G, Arnold M, Nedeltchev K, El-Koussy M. Plaque characteristics of asymptomatic carotid stenosis and risk of stroke. *Cerebrovasc Dis* 2012;34:343–350.
- Oviedo C, Maehara A, Mintz GS, Araki H, Choi SY, Tsujita K, Kubo T, Doi H, Templin B, Lansky AJ, Dangas G, Leon MB, Mehran R, Tahk SJ, Stone GW, Ochiai M, Moses JW. Intravascular ultrasound classification of plaque distribution in left main coronary artery bifurcations: Where is the plaque really located? *Circ Cardiovasc Interv* 2010;3:105–112.
- Prahl U, Holdfeldt P, Bergstrom G, Fagerberg B, Hulthe J, Gustavsson T. Percentage white: A new feature for ultrasound classification of plaque echogenicity in carotid artery atherosclerosis. *Ultrasound Med Biol* 2010;36:218–226.
- Ramnarine KV, Garrard JW, Dexter K, Nduwayo S, Panerai RB, Robinson TG. Shear wave elastography assessment of carotid plaque stiffness: *in vitro* reproducibility study. *Ultrasound Med Biol* 2014;40:200–209.
- Ramnarine KV, Hartshorne T, Sensier Y, Naylor M, Walker J, Naylor AR, Panerai RB, Evans DH. Tissue Doppler imaging of carotid plaque wall motion: A pilot study. *Cardiovasc Ultrasound* 2003;1:17.
- Reckless IP, Buchan AM. Stroke: Management and prevention. *Medicine* 2008;36:592–600.
- Reid DB. Carotid plaque characterization: helpful to endarterectomy and endovascular surgeons. *J Endovasc Surg* 1998;5:247–250.
- Reiter M, Bucek RA, Effenberger I, Boltuch J, Lang W, Ahmadi R, Minar E, Schillinger M. Plaque echolucency is not associated with the risk of stroke in carotid stenting. *Stroke* 2006;37:2378–2380.
- Ribbers H, Lopata RGP, Holewijn S, Pasterkamp G, Blankensteijn JD, De Korte CL. Noninvasive two-dimensional strain imaging of arteries: Validation in phantoms and preliminary experience in carotid arteries *in vivo*. *Ultrasound Med Biol* 2007;33:530–540.
- Ronen RR, Clarke SE, Hammond RR, Rutt BK. Carotid plaque classification: Defining the certainty with which plaque components can be differentiated. *Magn Reson Med* 2007;57:874–880.
- Saba L, Argiolas GM, Siotto P, Piga M. Carotid artery plaque characterization using CT multienergy imaging. *AJNR Am J Neuroradiol* 2013;34:855–859.
- Sabetai MM, Tegos TJ, Nicolaidis AN, El-Atrozy TS, Dhanjil S, Griffin M, Belcaro G, Geroulakos G. Hemispheric symptoms and carotid plaque echomorphology. *J Vasc Surg* 2000;31:39–49.
- Salem MK, Sayers RD, Bown MJ, West K, Moore D, Nicolaidis A, Robinson TG, Naylor AR. Patients with recurrent ischaemic events from carotid artery disease have a large lipid core and low GSM. *Eur J Vasc Endovasc Surg* 2012;43:147–153.
- Schaar JA, De Korte CL, Mastik F, Strijder C, Pasterkamp G, Boersma E, Serruys PW, Van Der Steen AF. Characterizing vulnerable plaque features with intravascular elastography. *Circulation* 2003;108:2636–2641.
- Schmitt C, Soulez G, Maurice RL, Giroux MF, Cloutier G. Noninvasive vascular elastography: toward a complementary characterization tool of atherosclerosis in carotid arteries. *Ultrasound Med Biol* 2007;33:1841–1858.
- Shi H, Mitchell CC, McCormick M, Kliewer MA, Dempsey RJ, Varghese T. Preliminary *in vivo* atherosclerotic carotid plaque characterization using the accumulated axial strain and relative lateral shift strain indices. *Phys Med Biol* 2008a;53:6377–6394.
- Shi H, Varghese T, Dempsey RJ, Salamat MS, Zagzebski JA. Relationship between ultrasonic attenuation, size and axial strain parameters for *ex vivo* atherosclerotic carotid plaque. *Ultrasound Med Biol* 2008b;34:1666–1677.
- Sztajzel R, Momjian S, Momjian-Mayor I, Murith N, Djebaili K, Boissard G, Comelli M, Pizolatto G. Stratified gray-scale median analysis and color mapping of the carotid plaque: Correlation with endarterectomy specimen histology of 28 patients. *Stroke* 2005;36:741–745.
- Teng Z, Sadat U, Huang Y, Young VE, Graves MJ, Lu J, Gillard JH. *In vivo* MRI-based 3-D mechanical stress–strain profiles of carotid plaques with juxtaluminal plaque haemorrhage: an exploratory study for the mechanism of subsequent cerebrovascular events. *Eur J Vasc Endovasc Surg* 2011;42:427–433.
- Widman E, Maksuti E, Larsson M, Bjällmark A, Caidahl K, D'hooge J. Shear wave elastography for characterization of carotid artery plaques: A feasibility study in an experimental setup. In: *Proceedings, IEEE International Ultrasonics Symposium, Dresden, Germany, 7–10 October 2012*. New York: IEEE; 2012.
- Zhao H, Zhao X, Liu X, Cao Y, Hippe DS, Sun J, Li F, Xu J, Yuan C. Association of carotid atherosclerotic plaque features with acute ischemic stroke: A magnetic resonance imaging study. *Eur J Radiol* 2013;82:e465–e470.